The Hg–H2 system: Potential energy surfaces of the lowlying states, reactivity of the 6s6p states of Hg on H2, classical dynamic study of Hg(3 P 1)+H2 half collision

A. Bernier and P. Millie

Citation: The Journal of Chemical Physics **88**, 4843 (1988); doi: 10.1063/1.454695
View online: http://dx.doi.org/10.1063/1.454695
View Table of Contents: http://scitation.aip.org/content/aip/journal/jcp/88/8?ver=pdfcov
Published by the AIP Publishing

The Hg–H_2 system: Potential energy surfaces of the low-lying states, reactivity of the 6s6p states of Hg on H_2, classical dynamic study of $Hg(^3P_1)+H_2$ half collision

A. Bernier and P. Millie
C.E.A./IRDI/DESICP-Département de Physico-Chimie, CEN/SACLAY, 91191 Gif-sur-Yvette Cedex, France

(Received 2 October 1987; accepted 21 December 1987)

Potential energy surfaces for HgH_2 have been calculated using a nonempirical relativistic effective core)potential incorporating configuration interaction by means of the CIPSI algorithm (configuration interaction by perturbation with multiconfigurational zeroth-order wave function selected by iterative process). Core-valence polarization and correlation energy are included via a perturbative treatment. Spin–orbit coupling is introduced through an effective Hamiltonian. These theoretical results are used to discuss the experimental ones for the $Hg(^3P_1) + H_2 \rightarrow HgH(X\,^2\Sigma^+) + H$ reaction. The different behaviors of the two van der Waals complexes are explained. Dynamical studies and classical trajectories calculations confirm that the dominant pathway is a direct dissociation on the first excited surface and is responsible for a highly peaked rotational distribution of the HgH product, in agreement with experiment.

INTRODUCTION

The $Hg(^3P_1) + H_2$ system has recently been studied experimentally by Breckenridge *et al.*[1] who carried out selective laser excitation of the van der Waals complex HgH_2. The two electronic configurations of the complex exhibit different behaviors. A theoretical evaluation of the potential energy surfaces is then required to explain these experimental results.

We use a relativistic effective core potential, which reduces the mercury atom to a two-electron system. The potential energy of the lowest states of the HgH_2 system has been calculated for about 300 different geometries with standard quantum chemistry methods.

A good evaluation of the topology of the potential energy surfaces (PES) is thus obtained and this allows discussion of the experimental results. Classical trajectories calculations on the present PES give us complementary informations on the reaction mechanisms.

I. SYMMETRY CONSIDERATIONS AND EXPERIMENTAL RESULTS

When the $Hg(^1S_0)\cdot H_2$ ground state complex prepared in a supersonic molecular beam is excited to the $Hg(^3P_1)\cdot H_2$ state, the molecular product HgH is readily detected. The two electronic configurations of the complex exhibit differents behaviors.

Before giving more details on theses two behaviors the labeling of the two configurations has to be explained. Because the spin–orbit coupling is very large in mercury, the Hund's case (c) must be used. In Table I the symmetry of the HgH_2 complex states correlated with $Hg + H_2(^1\Sigma_g^+)$ states at large Hg–H_2 distances are reported. In $C_{\infty v}$ geometry, the states are labeled with $\Omega = |L + S|$ which is a good quantum number.

At large Hg–H_2 distances, the excitation from $Hg(^1S_0)\cdot H_2$ into $Hg(^3P_1)\cdot H_2$ leads to two complex states: (i) A complex state of symmetry (0^+, A', A_1) in the $C_{\infty v}$, C_s, C_{2v} geometry. (ii) A complex state of symmetry $\Omega = 1$ in the $C_{\infty v}$ geometry. This complex is composed of two degenerate components (strictly degenerate at every distances Hg–H_2 in $C_{\infty v}$ geometry, approximately degenerate in C_s or C_{2v} geometry at large Hg–H_2 distances). These two components can be labeled ($\Omega = 1, A', B_2$) and ($\Omega = 1$, A'', B_1).

In terms of the Hund's case (a), the $Hg(^3P_1) + H_2$ complex is correlated to a $^3\Sigma^+$ and a $^3\Pi$ states in $C_{\infty v}$ geometry. When the spin–orbit coupling is added, the $^3\Sigma^+$ gives one $\Omega = 0^-$ state and one $\Omega = 1$ state, the $^3\Pi$ state gives: $\Omega = 0^+, \Omega = 0^-, \Omega = 1, \Omega = 2$ states. So we can see that the $\Omega = O^+$ complex state is correlated in Hund's case (a) only to the $^3\Pi$state. This complex state is referred to as the "Π complex state" by Breckenridge *et al.*[1] The $\Omega = 1$ state comes from the $^3\Sigma^+$ and the $^3\Pi$ states. It is referred to in the same paper as the "Σ complex state." In this paper, we have instead used the Hund's case (c) notation.

The experimental results of Breckenridge *et al.*[1] are then the following. The reaction pathway via the $\Omega = 0^+$ complex state is "direct," i.e., occurs within 0.1 ps. The rotational distribution of the product is peaked near $J = 19$. The reaction via the $\Omega = 1$ complex state is "indirect" and occurs on a time scale between 2 ps and 1 ns. The rotational distribution is bimodal, with a major component quite similar to

TABLE I. $Hg + H_2$ correlated states.

$Hg + H_2(^1\Sigma_g^+)$	$C_{\infty v}$	C_s	C_{2v}
$Hg(^1S_0)$	0^+	A'	A_1
$Hg(^3P_0)$	0^-	A''	A_2
$Hg(^3P_1^0)$	0^+	A'	A_1
$Hg(^3P_1^1)$	1	$A' + A''$	$B_2 + B_1$
$Hg(^3P_2^0)$	0^-	A''	A_2
$Hg(^3P_2^1)$	1	$A' + A''$	$B_2 + B_1$
$Hg(^3P_2^2)$	2	$A' + A''$	$A_1 + A_2$
$Hg(^1P_1^0)$	0^+	A'	A_1
$Hg(^1P_1^1)$	1	$A' + A''$	$B_2 + B_1$

 0021-9606/88/084843-12$02.10

the one resulting from the excitation of the $\Omega = 0^+$ complex and an additional minor component at low J.

No major isotopic effects have been noted in collision experiments at room temperature between Hg and H_2, D_2 or HD.[2]

Analogous results have also been obtained for "isoelectronic" systems. The internal energy distributions of CdH (CdD) produced in the reaction of $Cd(^3P_1)$ with H_2, D_2, and HD have been studied by Breckenridge *et al.*[3] Unusual, no isotope effects were observed, very similar to those reported for the reactions of $Zn(^3P_1)$[4] and $Hg(^3P_1)$,[1] and also for the reaction of $Mg(^1P_1)$ with H_2, D_2, and HD.[5]

II. METHODOLOGY

A. *Ab initio* calculations of PES

1. *General methodology*

The mercury atom is considered as a two-electron system with the use of a relativistic nonempirical effective core potential. Two component orbitals are derived from relativistic all-electron atomic calculations according to the method proposed by Barthelat, *et al.*[6] Nodeless one-component pseudoorbitals and corresponding pseudopotentials are obtained. Effective spin–orbit operators acting on pseudoorbitals are derived in order to reproduce the effect of the true spin–orbit operator on all–electron valence orbitals.[7] The Gaussian basis set used is a $5s5p3d$ set contracted to a $3s4p3d$ for mercury and a $5s2p$ contracted to $3s2p$ for hydrogen. The pseudopotentials parameters and the basis sets are reported in Ref. 8.

Configuration interaction was performed using the CIPSI algorithm with a three class selection of determinants.[9] Core-valence polarization is included via a second-order perturbative treatment.[10] Spin–orbit coupling is introduced through an effective Hamiltonian in a basis of LS states.[7]

The spectroscopic constants, binding energies and equilibrium distances for the low-lying states of the HgH molecule have been previously reported[8] and are in good accordance with the experimental results.

The potential energy for the HgH_2 system has been calculated for 300 different geometries in the C_{2v}, $C_{\infty v}$, C_s, and $D_{\infty h}$ symmetry groups.

2. *Molecular orbital set determination*

The perturbative calculations are relevant only if the energetic corrections are relatively small. This requires good zero-order wave functions to describe the states, and then a good start for representing molecular orbital sets.

A unique set of molecular orbitals cannot describe conveniently the states in very different geometries of the HgH_2 system. We have then partitioned the space in regions corresponding to different physical situations. A different molecular orbital set has been obtained for each region, in order to optimize the description of the first states of the HgH_2 system. The construction method of the molecular orbital set in the (C_{2v}, $r_1 = r_2 \leqslant 3.7$ a.u.) region is reported, for example, in Ref. 11.

With such elaborated molecular orbital sets, the generator space for the CIPSI algorithm includes less than 200 determinants, iteratively selected from various geometries. 1000 to 1500 determinants are considered up to infinite order of perturbation (variationally). The second order perturbation treatment recovers only 5% to 10% of the total correlation energy.

At the boundaries between two regions, we have to compare the potential energy obtained with the two different sets of molecular orbitals as a test of the quality of our calculations. In Table II are reported the energies obtained for the first states of the Hg–H–H system, in the following geometrical configuration: ($r_{HgH_1} = 3.10$ a.u., $r_{HgH_2} = 5.0$ a.u.) but obtained with molecular orbitals built in the three different ways: (i) from SCF and MCSCF calculations of the HgH_2 system, (ii) from the SCF occupied and virtual orbitals of the HgH^+ molecule and the H atomic orbitals, (iii) same as (ii), but for a slightly bent geometry (C_s, HgHH = 1°).

The difference between the two first calculations shows the quality of our calculations. The difference is smaller than 10^{-3} a. u. for the first states, and equal to some 10^{-3} for the higher states. These results emphasize the importance of a good choice of the molecular orbitals, as the higher states are not described as good as the lower ones on the starting molecular orbitals.

3. *SO coupling treatment*

The calculations are firstly done in a Hund's case (a) scheme. Spin–orbit coupling effect is then calculated through a perturbative treatment taking into account the configuration mixing.[7] This procedure gives us two kinds of information:

(1) The SO coupling elements between the eigenvectors of the electronic Hamiltonian without SO. Consequently, the SO coupling can be regarded as an additional coupling on the adiabatic potential curves previously obtained. These SO coupling elements allow the calculation of the transition probability between two states correlated through this coupling.

(2) The energies obtained after diagonalization of the $H_{el} + W_{SO}$ operator. The resulting adiabatic potential energy curves are readily obtained.

These two different treatments of the SO interaction have been used in this study. The SO coupling induces a large energy splitting only when the interacting states are closed.

TABLE II. Energies of the first states of Hg–H–H with r_1 (HgH) = 3.10 a.u. and r_2(HgH) = 5.0 a.u.

	OM(Hg–H–H) $IC + CV$	OM(HgH^+–H) $IC + CV$	C_s 1 deg $IC + CV$	
			A'	A''
$^1\Sigma^+$	− 2.167	− 2.167	− 2.167	
$^3\Sigma^+$	− 2.021	− 2.021	− 2.021	
$^3\Pi$	− 2.010	− 2.010	− 2.009	− 2.010
$^1\Pi$	− 1.975	− 1.972	− 1.970	− 1.971
$^1\Sigma^+$	− 1.960	− 1.957	− 1.956	
$^3\Sigma^+$	− 1.927	− 1.925	− 1.924	

For example, when the Hg–H_2 distance is very large, the entrance channel $Hg(^3P_1) + H_2$ must be considered with SO coupling because the interacting states are very close to each other. When the SO interacting states are sufficiently apart, the potential energy curves with SO are virtually degenerated with those without SO. We choose in that case the first approach and we present the potential curves without SO.

4. *Conclusion*

We evaluate to about 3.10^{-3} a.u. (0.1 eV) the average accuracy of our calculations. This is clearly smaller than the values of the wells and the activation barriers relevant in the present study and we conclude that the present HgH_2 PES are a good base for dynamical studies.

B. Classical dynamic studies

1. *Analytic fit of the PES.*

Classical dynamic studies require analytic expressions of the PES. The 300 *ab initio* PE values obtained for various geometries allow a good evaluation of the topology of the PES.

Specific PES must be reproduced in two dimensions: the linear Hg–H–H PES for the first $\Omega = 1$ state (see below) and the C_{2v} PES for the $^3B_2$ state, which are correlated to the entrance channel $Hg(^3P_1) + H_2$. We choose to construct a spline function from about 600 points interpolated from the equipotential figure, each of them being obtained with 50 to 100 *ab initio* energy calculations.

The two three dimensions PES of the ground state ($^1A'$) and of the first excited state ($^3A'$) have been reproduced using a polynomial function correlated to the diatomic potentials for large internuclear distances, following the method proposed by Murrell *et al.*[12]

A good quality of these analytic expressions is required for the classical trajectories studies but is difficult to obtain. For the $^3A'$ state, the topology of the surface is very rugged and we could not successfully reproduce correctly the PES for all geometrical configurations. However several physical considerations exposed later have helped us to simplify the problem. We choose to reproduce the entrance channel in the C_{2v} geometry and the C_s potential surface for a H–Hg–H angle greater than 45°. So, we calculate the classical trajectories first in the C_{2v} geometry for the entrance channel. Then, when the H–Hg–H angle is equal to 45°, we have slightly distorted the molecule and for various such "initial conditions" we pursue the calculations on the C_s surface. Details on this procedure are given later. Notice that considering the entrance channel in the C_{2v} geometry prevents us from studying the Hg + HD reaction.

2. *Classical trajectories calculations*

Classical trajectories calculations have been done with computer codes of C. Leforestier and A. Beswick. The Hamiltonian equations are solved with an Adams–Moulton predictor–corrector integrator with the restriction of a plane evolution.

Because the experiment has been done on jet-cooled species, we have made the calculations with H_2 populated rotational levels $J = 0$ and $J = 1$, which are the only occupied levels. We have also varied the collision energy (0 to 10^{-3} a.u.).

III. THE ENTRANCE CHANNEL OF THE $Hg(^3P_1)+H_2$ REACTION

In the first part of this paper, we focalize on the interpretation of the $Hg(^3P_1) + H_2$ half-collision reactions. But the knowledge of the potential energy surfaces gives several others informations that will be discussed in Sec. VII.

A. Approaches of Hg and H_2

The PES have first been obtained for large Hg–H_2 distances. Several qualitative considerations previously reported[11,13] let us guess the general features of the PES when the H–H distance is taken equal to the H_2 molecule equilibrium distance and the Hg–H_2 distance is decreasing. The calculated PES reported in Fig. 1 corroborate these considerations. In the C_{2v} geometry, the $^3B_2$ and the $^1B_2$ states are the only attractive states. The $^3B_2$ state exhibits an energy minimum of about 0.22 eV at a Hg–H_2 distance of 2.0 Å. In the $C_{\infty v}$ geometry, all the states are repulsive when the Hg–H_2 distance decreases.

The $^3B_2$–$^3A'$–$^3\Pi$ state is the first excited state of the HgH_2 system and is correlated to the entrance channel. The equipotential lines for a fixed H–H internuclear distance equals to 1.401 Å, are depicted in Fig. 2.

The free rotation of the H_2 molecule at large Hg–H_2 distances (i.e., the equilibrium distance of the van der Waals complex) disappears when the Hg–H_2 distance decreases. The rotation of the H_2 molecule is hindered and the C_{2v}

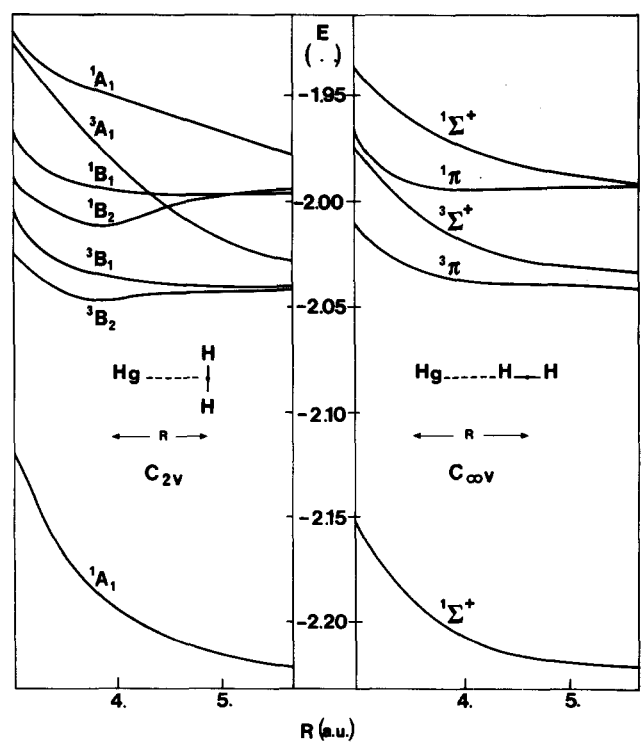

FIG. 1. The approach of Hg and H_2 in the C_{2v} and the $C_{\infty v}$ geometries.

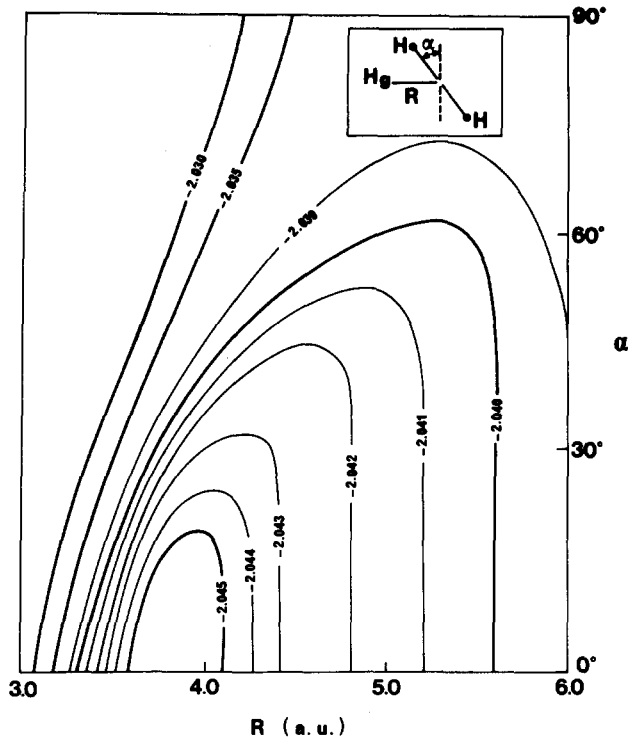

FIG. 2. Equipotential lines in a.u. of the first $^3A'$ state when d(H–H) = 1.401 a.u.

geometry (or C_s with an angle smaller than 20°) is preferred (the rotational energy for the $J = 1$ state of H_2 is about 10^{-3} a.u.). Classical trajectories calculations have shown that the H_2 molecule approaches the mercury atom from 6 to 4 a.u. in a time scale of 3 or 4000 atu. This large elapse of time compared to the free rotational period of the H_2 molecule (about 1000 atu) have led us to expect that the H_2 molecule can rotate during the Hg–H_2 approach and that the system is in a quasi-C_{2v} geometry at a distance of 4 a.u.

B. The Hg($^3P_1$)·H_2 complex at large distances

The $(\Omega = 0^+, A', A_1)$ complex is correlated in Hund's case (a) to the $(^3\Sigma^+, ^3A', ^3B_2)$ state. The C_{2v} or quasi-C_{2v} approach is then preferred for this complex state.

For the $(\Omega = 1, A'', B_1)$ component, correlated to the $^3B_2$ state in the C_{2v} geometry, the conclusion is the same as for the $(\Omega = 0^+, A', A_1)$ complex state. Nevertheless, the three states A', A_2, and B_1 resulting from the effect of SO coupling on the $^3B_2$ multiplet have different behaviors. At infinite Hg–H_2 distances, the B_1 state interacts with the B_1 state resulting from the $^3A_1$ state ($^3A_1 \rightarrow A_2, B_1, B_2$) and its energy is pulled down. But the $^3A_1$ state is very strongly repulsive (see Fig. 1) and this interaction decreases more rapidly than the stabilization due to the attractive electronic interaction between Hg and H_2 (attractive character of the $^3B_2$ state) when the Hg–H_2 distance decreases. The B_1 state is not yet stabilized. Consequently, at large Hg–H_2 distance, we have found a very small energy barrier for the B_1 state. This is in good qualitative accordance with the hypothesis offered us in the experimental paper.[14] Moreover, the translation–vibration coupling at such large distances is certainly small and a long time may be necessary to pass this small barrier. The $(\Omega = 1, A'', B_1)$ state is thus expected to react in the same way as the $(\Omega = 0^+, A', A_1)$ state in C_{2v} geometry but with a longer time scale.

The second component of the $\Omega = 1$ complex: i.e., $(\Omega = 1, A', B_2)$ is not correlated to the $^3B_2$ state in Hund's case (a), which is the only attractive state in the C_{2v} geometry. This B_2 state is correlated at relatively small distances with the $^3B_1$ state which is repulsive. In the $C_{\infty v}$ geometry, this $\Omega = 1$ state is correlated to the $^3\Pi$ state, which is less repulsive than the $^3B_1$ and the $^3A'$.

Then, we can conclude that two different geometrical approaches have to be carefully studied: Firstly, the C_{2v} geometrical approach and the evolution of the $^3B_2$ state, and secondly the $C_{\infty v}$ geometrical approach and especially the evolution of the $^3\Pi$ state which is correlated to the three components of the complex.

IV. THE $C_{\infty v}$ APPROACH

In Fig. 2 we have reported the potential curves for the Hg–H_2 approach keeping the H–H bond length equal to 1.401 a.u. In Fig. 3, we show the potential energy curves with a H–H bond length equal to 2.0 a.u. The major difference between these two figures is the relative position of the first $^3\Sigma^+$ state and the first $^3\Pi$ state. The inversion between these two states can be clearly observed in Fig. 4: the PE curves are shown with the first Hg–H distance fixed to 3.3 a.u. (the

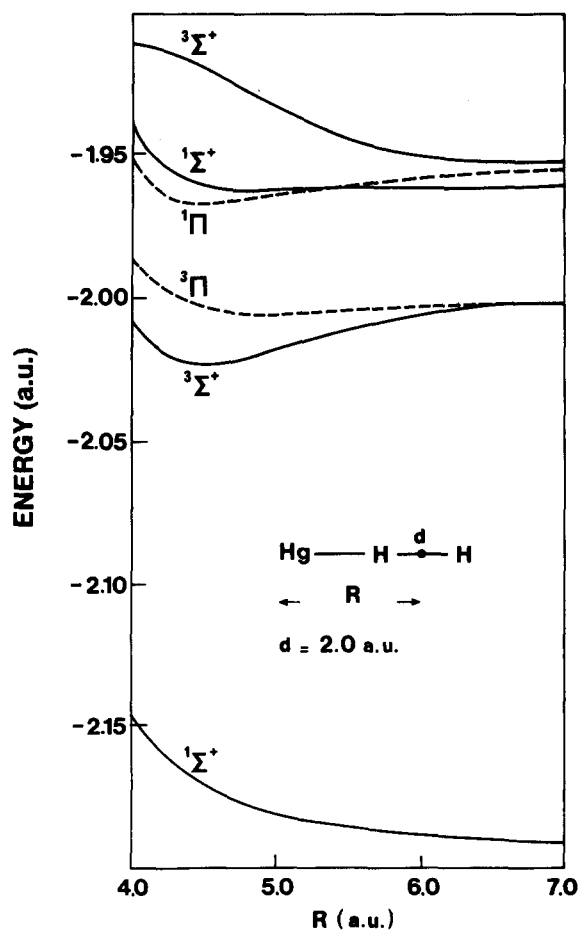

FIG. 3. The approach of Hg and H_2 in the C_{2v} geometry for the H–H distance equal to 2.0 a.u. Spin–orbit coupling not included.

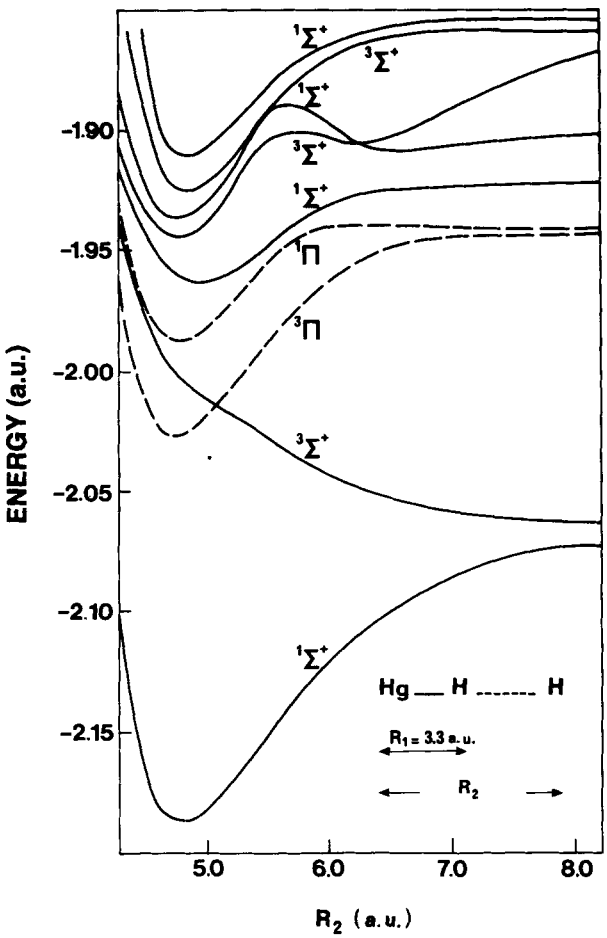

FIG. 4. Potential curves: Hg–H–H → HgH + H. Spin–orbit coupling not included.

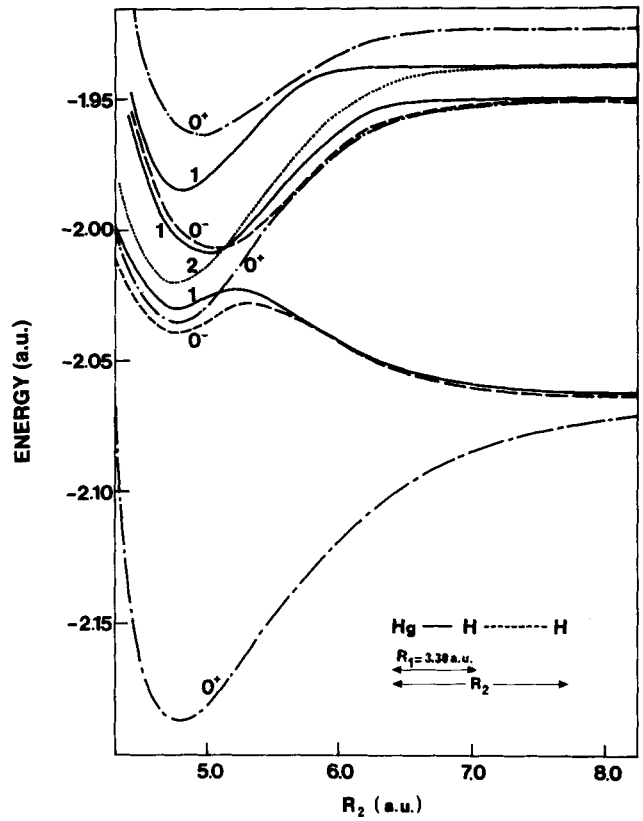

FIG. 5. Potential curves Hg–H–H → HgH + H. Spin–orbit coupling included.

equilibrium distance of the HgH molecule), and an increasing second Hg–H distance. When the spin–orbit coupling is added, the $^3\Sigma^+$ state leads to $\Omega = 0^-$, 1 and the $^3\Pi$ state leads to $\Omega = 0^+$, 0^-, 1,2. Thus, the resulting $\Omega = 1$ and $\Omega = 0^-$ states show an avoided crossing (see Fig. 5). We also notice that in the C_s — quasi-$C_{\infty v}$ geometry an avoided crossing between the two $^3A'$ states which correlate to the $^3\Pi$ and $^3\Sigma^+$ is observed even if SO is neglected.

The resulting activation barrier is small [0.62 eV at $d(\text{Hg–H}_1) = 1.85$ Å and $d(\text{H–H}) = 1.06$ Å] but greater than the energy of the $\text{Hg}(^3P_1)\cdot\text{H}_2(v = 0)$ complex. Therefore, the half-collision reaction from the $\Omega = 1$ complex state can lead to $\text{HgH}(X\,^2\Sigma^+) + \text{H}$ only by tunneling. The equipotential lines for the $\Omega = 1$ state in the $C_{\infty v}$ geometry are presented on Fig. 6.

Nevertheless, classical trajectories have been performed on the $\Omega = 1$ potential energy surfaces. Even with kinetic energy, so that the total energy is larger than the activation barrier, no reactive collision is evidenced. Conversely, the activation barrier can be overcome by vibrational energy and the reaction gives $\text{HgH}(X\,^2\Sigma^+) + \text{H}$ or $\text{Hg}(^1S_0) + \text{H} + \text{H}$ when we start from $\text{Hg}(^3P_1) + \text{H}_2(v = 1)$. Vibrational energy is then required to pass the activation barrier in classical calculations and for $\text{Hg}(^3P_1) + \text{H}_2(v = 0)$, a quantical tunneling effect is the only possible way to obtain a reactive collision. Such a tunneling effect can be responsible for the low J component of the rotational distribution energy experimentally observed for the $\Omega = 1$ complex state.

V. THE Hg–H_2 SYSTEM IN THE C_{2v} AND C_s GEOMETRIES

A. Generalities

The PE curves for large Hg–H_2 distances show that for the entrance channel of the $\text{Hg}(^3P_1) + \text{H}_2$ reaction, the C_{2v} geometry approach is favored. The free rotation of the hydrogen molecule is frozen.

For all these reasons, and because of the difficulties encountered in an attempt to obtain an analytic expression of the PES in the C_s geometry, we have studied the entrance channel in the C_{2v} geometry.

Classical trajectories in the C_{2v} geometry are done on the $^3B_2$ PES, the entrance channel of the $\text{Hg}(^3P_1) + \text{H}_2$ half-collision reaction, with the following initial conditions: (i) A Hg–H_2 distance of 11.3 a.u., i.e., the equilibrium distance of the van der Waals complex. (ii) An initial collision energy equal to zero. (iii) A cold rotational distribution, where the $J = 0$ and $J = 1$ states are the only occupied states of the H_2 molecule (ortho and parahydrogen).

Because of vibration–translation coupling, the distance between Hg and H_2 decreases, even with a zero initial collision energy. Nevertheless, the trajectory calculations are done with a collision energy of 10^{-4} a.u., which reduces the time of the approach and the one of the integration, and gives the same results as those obtained with a zero collision energy. A thousand trajectories have been calculated with different initial phases of H_2 vibration.

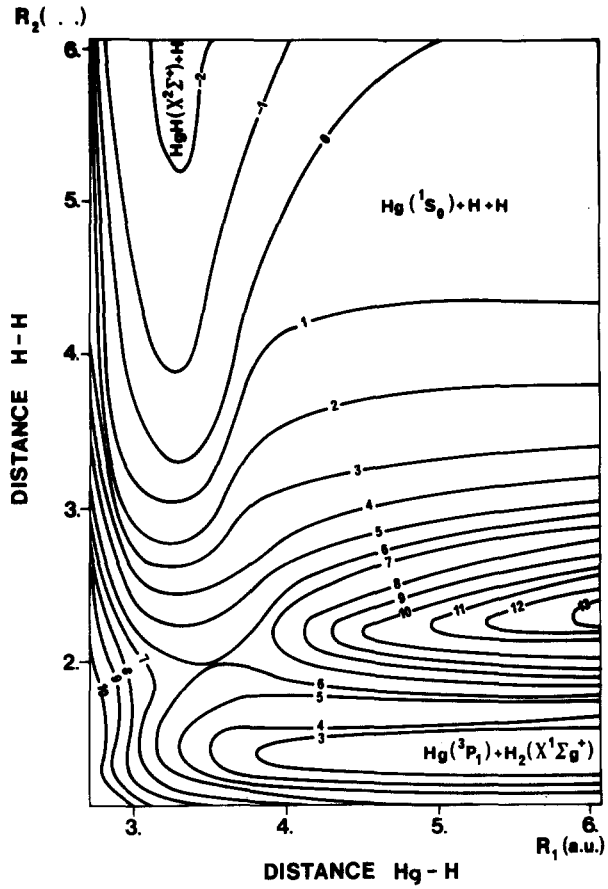

FIG. 6. Equipotential lines for the $\Omega = 1$ state in the $C_{\infty v}$ geometry. The zero equipotential line corresponds to the $Hg(^1S_0) + H + H$ energy ($-2.055\ 663$ a.u.). The distance between two equipotential lines is 0.005 a.u.

When the H–Hg–H angle equals 45°, the system is not yet in the entrance channel in which the C_{2v} geometry is favored. Its evolution must then be studied in C_s geometry. Moreover we can notice that in C_{2v} geometry, the system can lead to Hg + H_2 or Hg + H + H but not to HgH + H. This later channel, which is the major one, has then to be studied in the C_s geometry.

Starting with the velocities and positions of the atoms obtained from trajectories in the C_{2v} geometry in the entrance channel, we have tried to determine the velocities and positions for a HgH_2 system which would be at nearly the same position in a C_s geometry slightly different from the C_{2v} geometry. We have determined these "initial conditions" with the following procedure, starting from a C_{2v} system:

(a) The Hg middle point of the H–H bond is fixed and the hydrogen molecule is rotated at an angle equal to β, β being smaller than 20°.

(b) The H–H distance is increased in order to have the same potential energy for the new C_s system as for the C_{2v} system. For β varying between 0° and 20°, the H–H distance is increased by less than 20%.

(c) We assume that the relative velocity of the center of mass of the H_2 molecule with respect to the Hg atom is conserved.

(d) The relative velocities of the hydrogen atoms are calculated by writing the conservation of the total energy and the total angular momentum.

With these initial conditions, trajectories can be done in the C_s geometry on the $^3A'$ PES and on the $^1A'$ PES, as explained in details below.

These assumptions are physically reasonable. Moreover, we will see that the results of the trajectories calculations are not very sensitive to these initial conditions.

B. The two reaction pathways

1. *Through the ground state surface*

We have reported in Fig. 7 the PE curves of the HgH_2 system in the C_{2v} geometry for $r(Hg–H) = 3.10$ a.u. $= 1.64$ Å, where θ is the HHgH angle.

Molecular orbital correlations reported in Refs. 13 and 11 explain the strong activation barrier observed for the ground state. The $^3B_2$ state exhibits a minimum for $\theta = 70°$ and $r(Hg–H) = 3.8$ a.u., a strongly bent geometry. The equipotential lines for the $^3B_2$ state are reported in Fig. 8.

We observe in Fig. 7 that the $^1A_1$ potential curve crosses the $^3B_2$ one along a line represented by a dashed line in Fig. 8.

When we take into account the spin–orbit coupling, the $^1A_1$ state leads to a A_1 state, the $^3B_2$ state to A_1, A_2, B_1 states, as already mentioned. The two A_1 states show avoided cross-

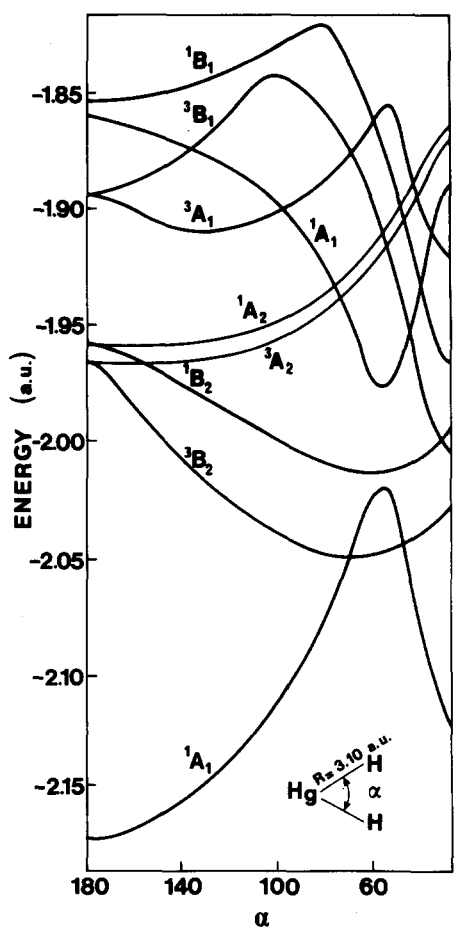

FIG. 7. Bending potential energy curves in the C_{2v} geometry. $d(Hg–H) = 3.10$ a.u.. Spin–orbit coupling not included.

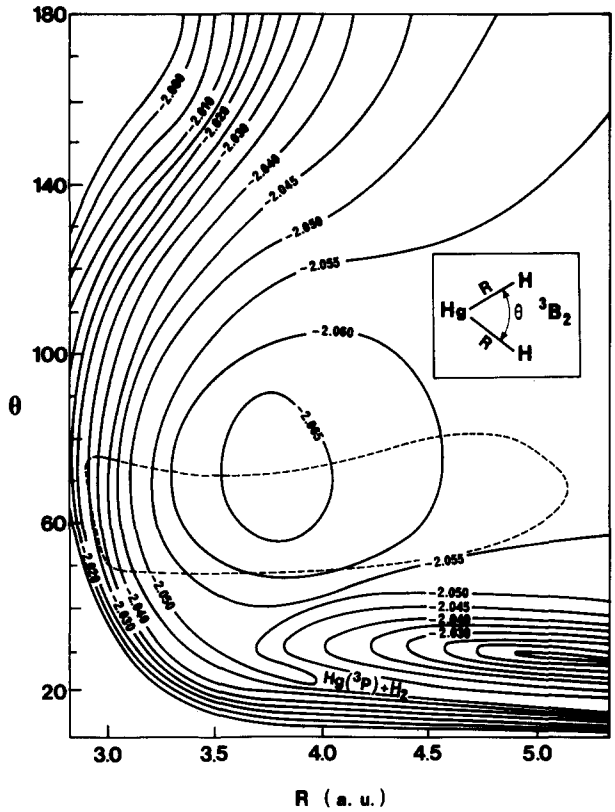

FIG. 8. Equipotential lines for the $^3B_2$ state. The energy values are in atomic units.

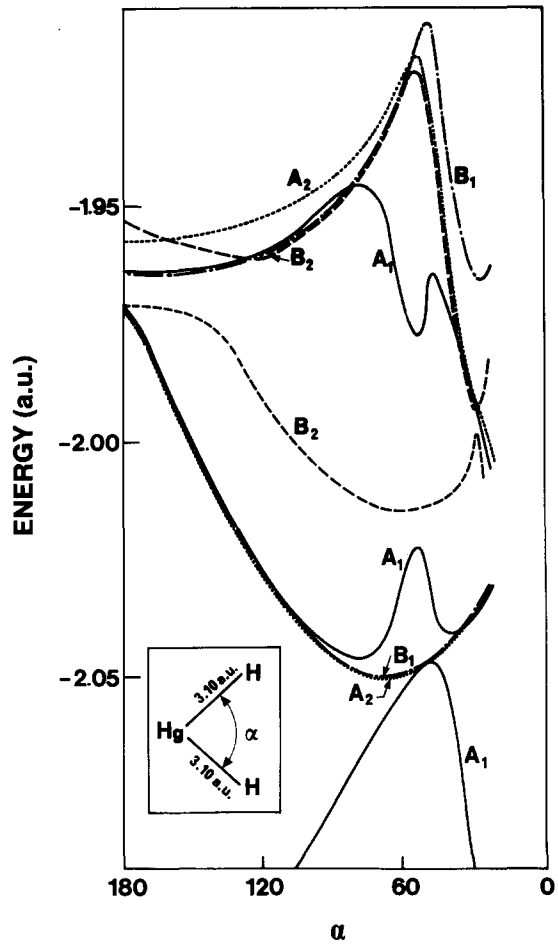

FIG. 9 Bending potential energy in the $C_{\infty v}$ geometry same as Fig. 7 but spin–orbit coupling included.

ing when adiabatic curves are depicted (see Fig. 9). The SO coupling can also be regarded as an additional coupling which can induce a transition between the $^3B_2$ state and the $^1A_1$ state.

Therefore, the $(\Omega = 0^+, A', A_1)$ component of the $Hg(^3P_1)\cdot H_2$ complex, correlated to this $^3B_2$ state is the only complex state (the other components of the complex having a symmetry different from the ground state's one) which may react on the PES of the ground state of the HgH_2 system. This ground state is correlated to the three fragments $Hg(^1S_0) + H + H$ limit and to the $HgH(X\,^2\Sigma^+) + H$ limit in the C_s geometry.

2. *On the first excited state surface*

In Fig. 10 are depicted the potential energy curves for the first states of the HgH_2 system as a function of θ, the H–Hg–H angle, and with $r_{HgH_1} = 3.10$ a.u. and $r_{HgH_2} = 4.0$ a.u.

When one Hg–H distance increases, the PE curves get close to the ones of the HgH + H system: two merged lines correlated to the singlet and triplet configurations obtained from $HgH(X\,^2\Sigma^+) + H(^2S)$. The PE curves for $r_{HgH_1} = 3.10$ a.u. and $r_{HgH_2} = 6.0$ a.u. are depicted in Fig. 11.

When $\theta = 0°$, the PE curve in situations where $r_{HgH_1} = 3.10$ a.u. and r_{HgH_2} increases have been reported in Fig. 4. The PE curves for $\theta = 180°$, $r_{HgH_1} = 3.10$ a.u. and increasing r_{HgH_2} are reported in Fig. 12. In Fig. 13 are reported the equipotential lines of the $^3A'$ state when $r_{HgH_1} = 3.10$ a.u., as a function of r_{HgH_2} and θ = H–Hg–H.

The topology of the PES is such that the strongly bent H–Hg–H molecule formed in the C_{2v} geometry can dissociate in the C_s geometry into HgH + H without any activation barrier, with a H–Hg–H angle approximatively equal to 70°. This pathway is expected to lead to a rotationally excited HgH fragment because of the strong anisotropy of the PES. The reaction is expected to occur through a strongly bent HHgH molecule, in which the H–H bond is broken [d(H-H) = 3.5 a.u.] before one hydrogen atom departs and so the HgH product is formed. This may explain the lack of isotopic effects found experimentally (same HgH rotational distribution for Hg + H_2 and Hg + HD).

In conclusion, these two different pathways can lead to HgH from $Hg(^3P_1)\cdot H_2$ in the C_{2v} and the C_s geometries. However, we believe that the direct dissociation on the excited surface is the more plausible pathway: for the $(\Omega = 1, A'', B_1)$ complex state, this is the only possible pathway; for the $(\Omega = 0^+, A', A_1)$ complex state, the transition to the ground state is possible but as the rotational HgH distribution for this complex state is very similar to the $\Omega = 1$ one, we can expect that the same mechanism occurs for the two complex states. However, more precise information on the mechanism requires dynamical studies.

C. Dynamical studies

1. *On the ground state potential energy surface*

Firstly, we have evaluated the probability of the transition from the $^3B_2$ ($^3A'$) state to the $^1A_1$ ($^1A'$) state.

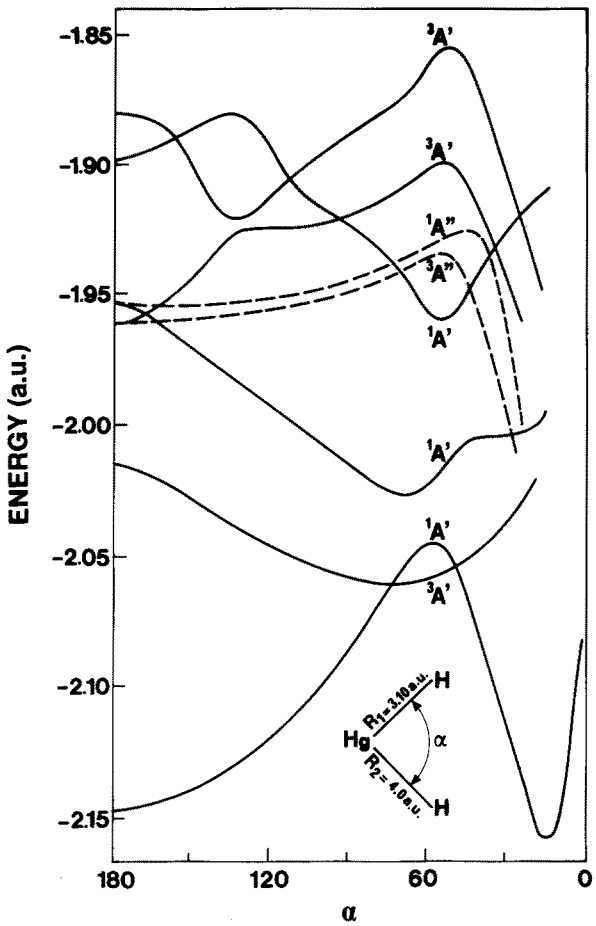

FIG. 10. Bending potential energy curves: r_1(Hg–H) = 3.10 a.u., r_2(Hg–H) = 4.0 a.u.

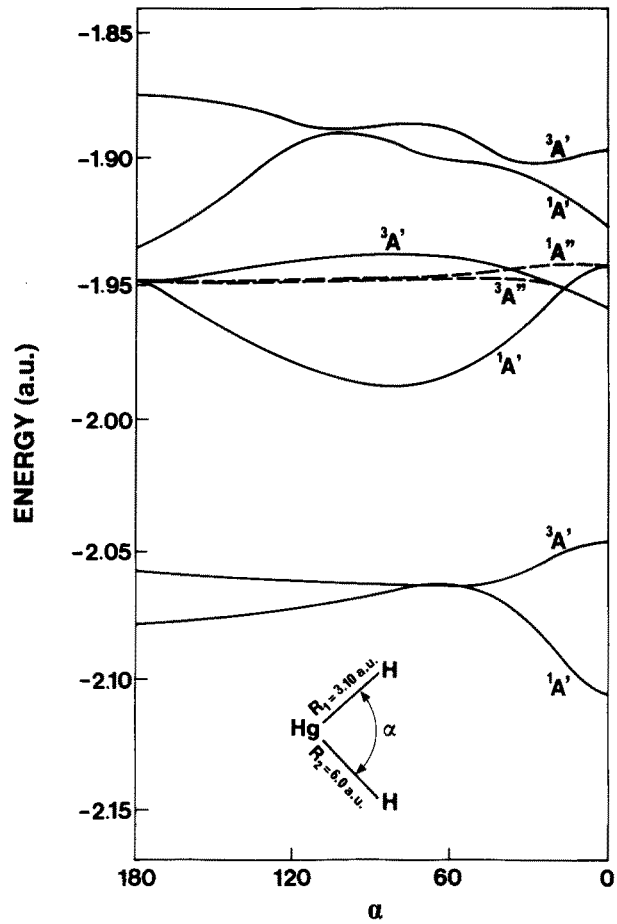

FIG. 11. Bending potential energy curves: r_1(Hg–H) = 3.10 a.u., r_2(Hg–H) = 6.0 a.u.

We have then performed classical trajectories calculations in the C_{2v} geometry for the entrance channel. Then, we have studied the evolution of the system on the $^3A'$ surface in C_s geometry, and we stop the trajectory at the crossing point between the $^1A'$ and the $^3A'$ surfaces. We can evaluate at this crossing point the transition probability with the Landau–Zener formula. The mean probability obtained is about 10^{-4} or 10^{-5}. Discussion of the different factors shows that in all cases, this probability should be less than 10^{-3}. Therefore, this is probably not the dominant reaction mechanism. Nevertheless, we can study what would be the evolution of the system on the $^1A'$ PES from these crossing points.

A very large number of these trajectories leads to the formation of $Hg(^1S_0) + H_2(v)$, i.e., inelastic collisions, through two mechanisms: (i) If the transition to the $^1A'$ PES occurs at a "first type crossing point" (H–Hg–H angle approximatively equal to 50°, see Fig. 8), the bent HgH_2 molecule is in front of a wall of potential. The two hydrogen atoms are pushed back in their incoming direction: the H–Hg–H angle decreases and the Hg–H distances increase. An inelastic collision is predicted with high values of the vibrational and rotational energies of the H_2 molecule. (ii) The bent HgH_2 molecule has a strong propensity to increase the H–Hg–H angle because of the velocities of the hydrogen atoms. If the transition to the $^1A'$ PES occurs at a "second type crossing point," (i.e., θ = H–Hg–H greater than 70°),

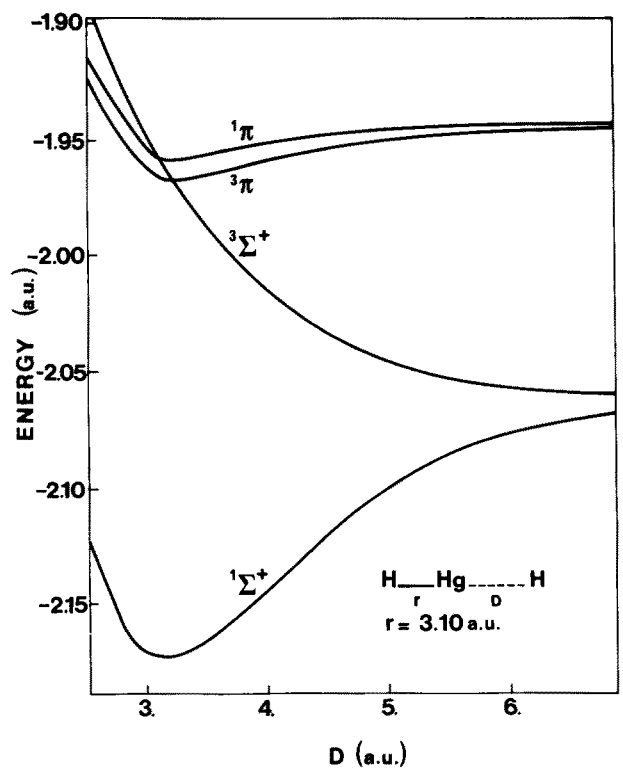

FIG. 12. The abstraction reaction H–Hg–H → HgH + H. Spin–orbit coupling not included.

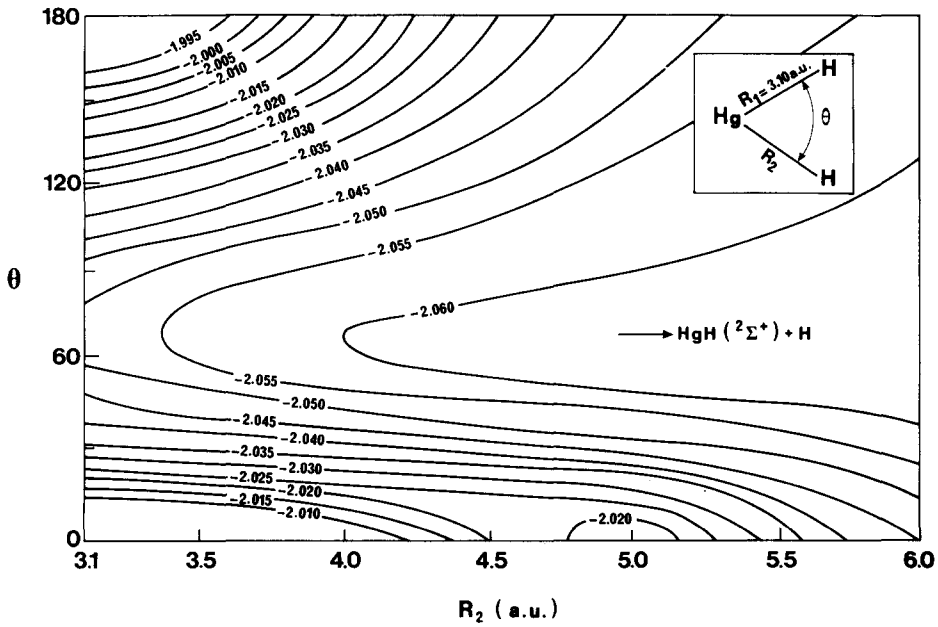

FIG. 13. Equipotential lines for the $^3A'$ state. $r_1(\mathrm{HgH}) = 3.10$ a.u.

the H–Hg–H angle increases and the Hg–H distances too, because of the topology of the $^1A'$ PES. The H–Hg–H angle becomes greater than 180°, and the molecule bends on the other side. The Hg–H bonds are broken and the H–H bond is formed again. A rotationally and vibrationally excited H_2 molecule is obtained. This kind of reaction can also be observed if the transition occurs at a first type crossing point, because when theHg–H distances increase, the wall vanishes and the H–Hg–H angle can increase (see Fig. 10).

Some trajectories lead to the formation of HgH with a mechanism similar to the second one. The distortion of the molecule is larger and one of the two Hg–H bonds is not broken, whereas the second hydrogen atom departs. The rotational distribution of the HgH fragment we obtain is quite flat. We have especially obtained large values ($J = 30$) of the angular momentum which are not experimentally observed.[1]

Two typical examples of trajectories from a first type crossing point are reported in Figs. 14 and 15.

In conclusion, we have three arguments to think that the formation of the HgH molecule in the half-collision reaction of $\mathrm{Hg}(^3P_1)$ and H_2 does not occur via a transition to the ground state potential energy surface. These reasons are:

(i) The transition probability at the $^3A'$–$^1A'$ crossing point is very small.

(ii) The two van der Waals complexes give similar rotational distributions but only one of them may react through a transition to the ground states PES.

(iii) The rotational distribution resulting from our trajectories calculations on the ground state PES is very different of the experimentally observed one.[1]

2. *On the first excited state potential energy surface*

The rotational distributions for the HgH fragment obtained in the reaction $\mathrm{Hg}(^3P_1) + H_2 \rightarrow \mathrm{HgH} + \mathrm{H}$, on the first excited state surface $^3A'$, for $J_{\mathrm{total}} = 0$ and $\beta = 5°$, 10°, 15°, 20° are reported in Fig. 16. The rotational distribution is peaked at $J = 19$. This result is in very good accord with the experimentally observed rotational distributions.[1]

Several remarks have to be made: (i) The rotational distributions obtained for $\beta = 5°$, 10°, 15°, and 20° have been added in Fig. 16. This is a crude approximation: the angular distribution at the end of the entrance channel has no reason to be flat. But because of the approximation made in considering the entrance channel only in the C_{2v} geometry, we cannot determine the true angular distribution. Nevertheless, the rotational distribution obtained for the different values of β are very similar (see Table III). Whatever is the real angular distribution, we can conclude that the rotational distribution of the fragment HgH is peaked at about $J = 19$. (ii) Very similar rotational distributions are obtained for the

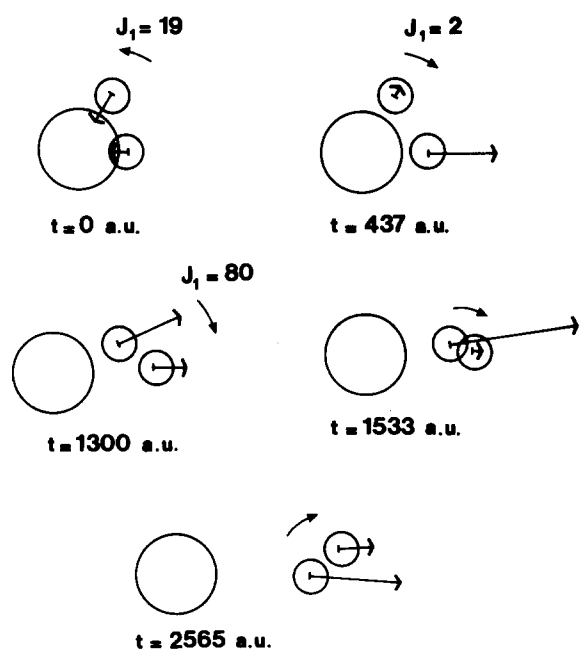

FIG. 14. Example of trajectory on the ground state surface leading to an inelastic collision.

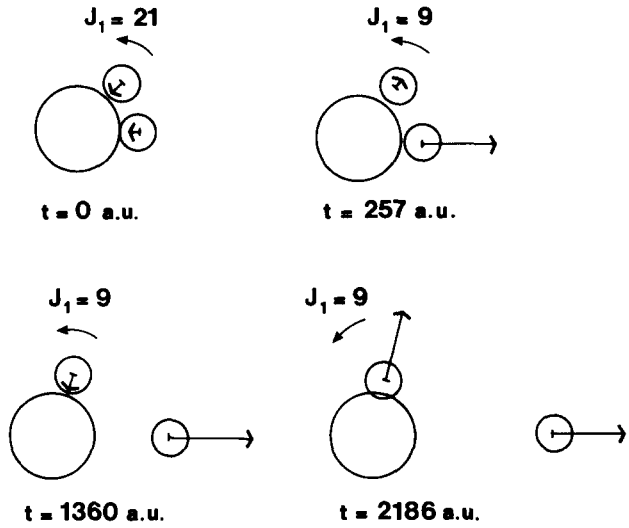

FIG. 15. Example of trajectory on the ground state surface leading to the formation of the mercury hydride molecule.

different vibrational levels of HgH. This allows the addition of the distributions for all vibrational levels which has been made in Table III. This result explains the strong similarity between the rotational distribution for the $v=0$ and the $v=1$ levels of HgH observed by Bras *et al.*[2] for $Hg(^3P_1)$ and H_2 collision reaction. (iii) Such a peak $J=19$ rotational distribution is also obtained: When we modify the value of the relative kinetic energy of particles during the approach between the mercury atom and the mass center of the hydrogen molecule (with a constant total energy) when the geometry is changed from C_{2v} to C_s; for larger initial collision energy (10^{-3} a.u.). This explains why Bras *et al.*[2] have observed in collision experiments the same rotational distribution as Breckenridge *et al.*[1] in half-collision experiments; for $J_{H_2}=1$. The existence of ortho and para hydrogen in the H_2 gas does not have influence on the rotational distribution of HgH. (iv) For small values of β (between 0° and 5°), the geometry is very close to C_{2v} and, for $J_{H_2}=0$, the products

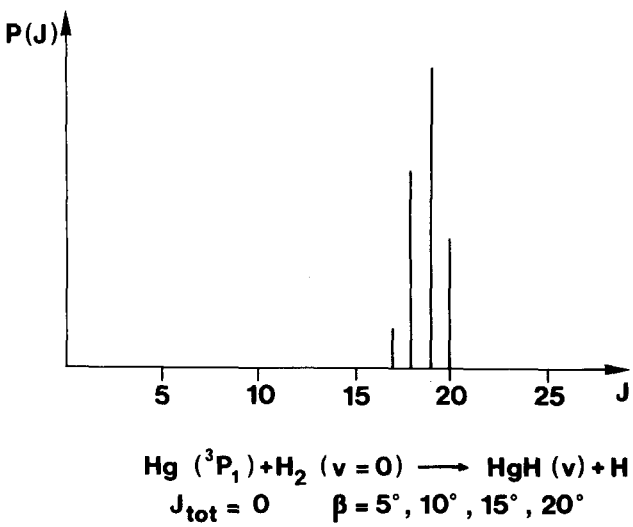

FIG. 16. Rotational distribution of the HgH molecule produced in the $Hg(^3P_1)$ and H_2 collision reaction.

TABLE III. Percentage of trajectories leading to the different values of J as a function of the β angle.

%	5°	19°	15°	20°
$J\leqslant 15$	0	0	0	0
$J=16$	7	1	1	1
$J=17$	77	6	6	6
$J=18$	9	8	7	79
$J=19$	0	83	83	14
$J=20$	0	2	3	0
$J\geqslant 21$	0	0	0	0

are mainly Hg + H + H or HgH + H but with HgH vibrationally very excited (for $J_{H_2}=1$, HgH can be obtained without large vibrational energy). The rotational distributions for these small values of β are different from the previous ones reported. They are not so peaked and we obtain J values between 4 and 16. This probably explains the tail of the distribution at small values of J experimentally observed. The mechanisms which give these two types of distributions are different. In the first case ($\beta>5°$), the molecule is asymmetric and one of the Hg–H bonds is very rapidly broken. An example of such a mechanism is given in Fig. 17. In the second case ($\beta<5°$), the Hg–H bond is not broken so rapidly and vibrates at first. The bond is broken for a larger H–Hg–H angle value and then gives an angular momentum smaller than in the first case. An example of such a trajectory is given in Fig. 18.

D. Isotopic complexes Hg·D_2

The rotational distribution of HgD produced by the $Hg(^3P_1)$ and D_2 collision has been obtained in the same way. The rotational distribution is more dependent on the β angle than for the HgH_2 complex study. So, as we cannot determine the angular distribution, we cannot give a good estimation of the rotational distribution of HgD. Significant differences can nevertheless be noticed. The calculated rotational distribution is smoother, small values of J are obtained and also larger values ($J\approx 30$). The maximum of the distribution is obtained for larger values than $J=19$ obtained for H_2. All these trends are in good accord with the experimental HgD rotational distribution observed by Bras *et al.*[2]

VI. CONCLUSION: REACTIVITY OF $Hg(^3P_1)$ WITH H_2

The first complex is correlated to $Hg(^3P_1^0)$ and is referred to as $(\Omega=0^+, A', A_1)$. This complex state dissociate from a strongly bent H–Hg–H molecule in HgH + H or Hg + H + H on the first excited state surface and the HgH

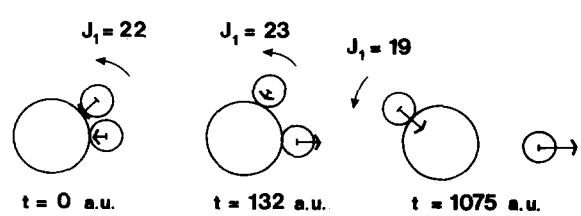

FIG. 17. Example of trajectory on the first excited state surface $Hg + H_2(v=0, J=0) \rightarrow HgH(v=1) + H$; $\beta=10°$.

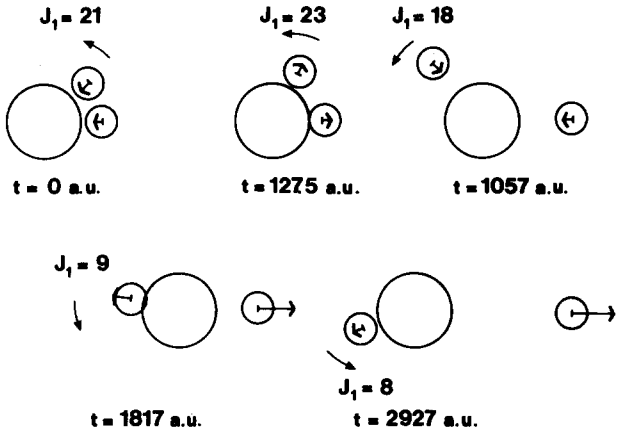

FIG. 18. Example of trajectory on the first excited state surface. $Hg + H_2(v=0, J=0) \rightarrow HgH(v=1) + H; \beta = 1°$.

rotational distribution calculated for the fragment HgH is peaked at $J = 19$, in good accordance with the experimental results.

The second van der Waals complex is correlated to the two $Hg(^3P_1^1)$ components, strictly degenerated in the $C_{\infty v}$ geometry, and quasidegenerated at large Hg–H_2 distances in the C_s and C_{2v} geometries. These two components react differently.

The $(\Omega = 1, A', B_2)$ component reacts in $C_{\infty v}$ (or quasi-$C_{\infty v}$ geometry) by a tunneling effect through a little activation barrier. The HgH molecule is probably obtained in this case with little rotational energy.

The $(\Omega = 1, A'', B_1)$ component is correlated at short Hg–H_2 distances with the $^3B_2$ state [in Hund's case (a)] and is virtually degenerated with the A_1 (in C_{2v}) state correlated to the $(\Omega = 0^+, A', A_1)$ complex state. This component reacts in the same way as this $\Omega = 0^+$ complex state, on the first excited surface and gives the same peaked rotational distribution. But a small activation barrier exists in the entrance channel and is probably reponsible for the larger lifetime of the complex.

These two components of the $\Omega = 1$ complex are then responsible of the bimodal rotational distribution experimentally observed.

VII. COMPLEMENTARY RESULTS

A. The formation of the HgH_2 molecule

The ground state potential energy surface of the HgH_2 system exhibits a minimum in the symmetric ($D_{\infty h}$) linear geometry with a Hg–H distance of 3.10 a.u. (1.64 Å). The mercury dihydride molecule is then a bound species with a dissociation energy of 3.15 eV. The calculation of the vibrational frequencies give $\nu_1 = 2006\ cm^{-1}$, $\nu_2 = 512\ cm^{-1}$, and $\nu_3 = 2271\ cm^{-1}$.

The formation of this HgH_2 molecule is rather difficult. As we can see in Fig. 7, the formation of this inserted component is highly endothermic from $Hg(^1S_0) + H_2$. This formation is energetically possible from $Hg(^3P_1) + H_2$, with a transition at a crossing point to the ground state potential energy surface $^1A_1$.

The analogous MgH_2 molecule has been experimentally observed in rare gas matrix from $Mg(^1P_1) + H_2$.[5] The ($^1B_2$–$^1A'$) PES correlated to the entrance channel crosses the PES of the ground state.[13] In the C_s geometry, the $^1A'$ states are electronically coupled which allow the formation of the ground state of the MgH_2 molecule. The existence of an efficient vibrational relaxation channel in the matrix explains the formation of the linear inserted product MgH_2.

Such a reaction may occur in matrix and leads to the formation of HgH_2 from $Hg(^3P_1) + H_2$. But a major difference with MgH_2 comes from the nature of the coupling between the entrance channel surface and the ground state surface. For magnesium, these PES are $^1A'$ in C_s-quasi C_{2v} geometry. For mercury, these PES are $^3A'$ for the excited state and $^1A'$ for the ground state. These two PES are coupled only by spin–orbit interaction and the transition probability previously calculated is very small. Moreover, the $^1A'$ PES correlated to the $Hg(^1P_1) + H_2$ does not cross the ground state PES and a mechanism similar to the magnesium case is impossible. This may explain why the linear inserted product HgH_2 has not yet been experimentally observed.

B. Reactivity of $Hg(^3P_0)$ with H_2

$Hg(^3P_0) + H_2$ is correlated in the C_{2v} geometry to the first A_2 state, resulting from the $^3B_2$ multiplet in Hund's case (a), and in the C_s geometry to the $\Omega = 0^-$ state. Two different pathways are possible: (i) a direct dissociation in the C_s-quasi C_{2v} geometry on the first excited PES, leading to formation of HgH + H and Hg + H + H, (ii) a reaction in the $C_{\infty v}$ geometry with a tunneling effect.

The PES of the $\Omega = 0^-$ state is similar to the $\Omega = 1$ PES (Fig. 5). But the C_{2v} approach is favored and the $C_{\infty v}$ reaction would be slower. The first pathway is probably the dominant one. Experimental work on this $Hg(^3P_0) + H_2$ system would be of great interest, especially the knowledge of the HgH rotational distribution. The A_2–A'' correlated PES is not coupled with the ground state PES, and a similar rotational distribution to the one observed from $Hg(^3P_1) + H_2$ would confirm our previously reported conclusions.

C. Reactivity of $Hg(^3P_2)$

The states correlated to $Hg(^3P_2)$ are repulsive at large Hg–H_2 distances for all symmetries. Moreover, they are not correlated with $HgH(X\,^2\Sigma^+) + H$ or $Hg(^1S_0) + H + H$. The excited states of these products are energetically inaccessible.[8] The $Hg(^3P_2)$ van der Waals complex is then probably not reactive, at least if no hyperfine structure transition occur at large internuclear distance.

D. Reactivity of $Hg(^1P_1)$

The $^1B_2$ state is the only attractive state correlated to $Hg(^1P_1) + H_2$ but this state is correlated to $HgH(^2\Pi_{1/2}) + H$, and this exit channel is not energetically accessible. As no crossing point with the ground state PES has been observed in our calculations, conversely with $Mg(^1P_1)$,[13] this state has no exit channel, except in the case

of hyperfine coupling between quasiparallel PES or spontaneous fluorescence on the ground state. Notice that this may be the easiest way to observe the formation of the HgH_2 molecule.

E. Analogous systems

The major conclusion obtained for the $Hg(^3P_1) + H_2$ collision is that the formation of HgH occurs on the first excited surface and not through a transition to the ground state surface. This is a different conclusion from those previously postulated by Breckenridge *et al.* for reactions of $Hg(^3P_1)$,[1] $Mg(^1P_1)$,[5] $Zn(^3P_1)$,[4] and $Cd(^3P_1)$[3] with H_2. For $Mg(^1P_1)$, the electronic coupling between the ground state and the $^1A'$ state correlated to the entrance channel is stronger than spin–orbit coupling in the mercury case. The transition to the ground state is much more likely and the reaction can occur through the formation of the inserted linear product H–Mg–H, which is confirmed by the observation of the magnesium dihydride molecule in rare gas matrices from $Mg(^1P_1) + H_2$.[15]

For Zn and Cd the spin–orbit parameter is smaller than for the mercury atom, so we think that the reaction most probably occurs in the same way as for mercury atom, on the first excited surface.

VIII. CONCLUSION

Relativistic pseudopotentials and standard quantum chemistry methods have been used to describe the mercury atom as a two-electron system. The potential energy surfaces of the HgH_2 system have been calculated and the experimentally observed reactivity of the $Hg(^3P_1)\cdot H_2$ van der Waals complexes has been discussed. The pathway deduced from the topology of the PES has been confirmed by classical trajectories studies which have given qualitatively good results. A more precise dynamical work would be of interest for a detailed study of isotopic effects, but our approximate study already explains satisfactorily the major experimental observations.

ACKNOWLEDGMENTS

The authors thank A. Beswick and C. Leforestier for making available to us their computers codes for classical trajectory calculations, and also B. Soep and C. Jouvet for helpful discussions, and I. Nenner for reading the manuscript.

[1] W. H. Breckenridge, C. Jouvet, and B. Soep, J. Chem. Phys. **84**, 1443 (1986).
[2] N. Bras, J. Buteaux, J. C. Jeannet, and D. Perrin, J. Chem. Phys. **85**, 280 (1986).
[3] W. H. Breckenridge, H. Umemoto, and J. H. Wang, Chem. Phys. Lett. **123**, 23 (1986).
[4] W. H. Breckenridge and J. H. Wang, Chem. Phys. Lett. **123**, 17 (1986).
[5] W. H. Breckenridge and H. Umemoto, J. Chem. Phys. **75**, 698 (1981); W. H. Breckenridge and J. H. Wang, Chem. Phys. Lett. **137**, 195 (1987).
[6] J. C. Barthelat, M. Pelissier, and Ph. Durand, Phys. Rev. A **21**, 1773 (1980).
[7] C. Teichteil, M. Pelissier, and F. Spiegelmann, Chem. Phys. **81**, 273 (1983).
[8] A. Bernier, Ph. Millie, and M. Pelissier, Chem. Phys. **106**, 195 (1986); in Table I, read for the *d* pseudopotential parameter: + 12.310 353 instead of − 12.310 353.
[9] S. Evangelisti, J. P. Daudey, and J. P. Malrieu, Chem. Phys. **75**, 91 (1983).
[10] G. H. Jeung, J. C. Barthelat, and M. Pelissier, Chem. Phys. Lett. **91**, 81 (1982).
[11] A. Bernier and Ph. Millie, Chem. Phys. Lett. **134**, 245 (1987).
[12] *Molecular Potential Energy Functions* edited by J. N. Murrell, S. Carter, S. C. Farantos, P. Huxley, and J. C. Varandas (Wiley, New York, 1984).
[13] P. Chaquin, A. Sevin, and H. Yu, J. Phys. Chem. **89**, 2813 (1985).
[14] C. Jouvet, Thèse de doctorat d'état, Université de Paris-Sud, Orsay, 1985.
[15] J. C. McCaffrey, J. M. Parnis, G. A. Ozin, and W. H. Breckenridge, J. Phys. Chem. **89**, 4945 (1985).